ADAPTIVE ℓ_0-NORM SPARSE THIRD ORDER VOLTERRA FILTER FOR TRANSCRANIAL ULTRASOUND IMAGE ENHANCEMENT: *IN-VIVO* RESULTS

James Cunningham *, Thyagarajan Subramanian **, Mohamed Almekkawy *

*DSchool of Electrical Engineering and Computer Science, Penn State University, University Park, PA 16802
** Department of Neurology, Penn State University, Hershey, PA 17036
[jdc5549, tus16, mka9] @psu.edu

ABSTRACT

Differentiating between the early stages of Parkinson's Disease (PD) and other diseases with parkinsonian symptoms is difficult from analyzing motor degeneration symptoms alone. For this reason, a commonly used diagnostic marker for PD is the hyperechogenicity of the Substantia Nigra (SN), which can help to make an early differential diagnosis of PD. Current practice for determining if an image displays hyperechogenicty relies on clinician experience heavily because of the difficulty of discerning features in standard B-mode imaging. Harmonic imaging has been studied extensively, and while it does improve the image quality, it suffers from spectral overlap with the noisy fundamental component. Our approach uses an adaptive Third Order Volterra Filter (ToVF), which avoids this problem by completely separating an image into its linear, quadratic, and cubic components with no overlap. One of the standard implementations of the ToVF is through an adaptive Recursive Least Squares (RLS) algorithm. This paper examines two algorithms developed through applying an ℓ_0 constraint on the standard RLS cost function. The two algorithms approximate this cost function in different ways, one using a Slow Time Varying (STV) approximation and the other using a Taylor Series Expansion (TSE) approximation. Theoretically the ℓ_0 constraint will shorten the number of iterations to reach steady state without sacrificing image quality. Our results confirm that these theoretical results hold on an *in vivo* application.

1. INTRODUCTION

Hyperechogenicity of the SN has been shown to be useful in the differential diagnosis of idiopathic Parkinson's Disease (iPD) and atypical parkinsonian syndromes such as multiple system atrophy, progressive supranuclear palsy, and corticobasal degeneration, because at the early stages of these diseases motor degeneration symptoms can appear very similar [15]. SN hyperechogenicity is also considered risk marker in prodromal PD, as it can manifest before the first symptoms appear [14]. Hyperechogencity is diagnosed by manually outlining the echogenic area of an ultrasound image, and if the area is above a threshold value of $0.2\,cm^2$, it is considered hyperechogenic [2]. Additionally, the reliability and reproducibility of results for SN hyperechogenicity has been shown to be highly dependent on clinician experience, in large part because the images often contain noise and image artifacts which can obscure the echogenic area [3]. This motivates some way to improve the quality of the image so there is less ambiguity for someone who has not dealt with hundreds of SN ultrasound images. Ultrasound imaging is particularly well-suited in detecting echogencity. Transcranial B-mode ultrasound imaging is able to capture and delineate major brain structures including the "butterfly shaped" midbrain, third and lateral ventricles, basal cisterns in monkeys [1], and other studies have shown that applying Transcranial Ultrasound Imaging (TCUI) to the human brain results in visible SN hyperechogenicity [2]. The Volterra filter offers advantages in detecting the small nonlinear echo components from the received images and extracting noise components within the signal by rejecting the additive Gaussian noise [4]. A post beamforming ToVF has been shown to separate an ultrasound image into its fundamental, second, and third harmonic components with the aid of micro-bubble ultrasound contrast agents [5]. Sound waves inside tissue media preserve this nonlinear property found in micro-bubbles that allows harmonic images to show improved image quality. Although the Volterra filter has a non-linear input-output relationship, its coefficients display a linear relationship, which makes it possible to compute the Volterra kernels through linear processing. When implementing adaptive LMS with an SoVF [7] or recursive least squares algorithm with ToVF [4], nonlinear components of the image usually contain higher dynamic and contrast range than normal B-mode images.

Our previous work investigates the use of Least Mean Squares (LMS) algorithm variants, including sparse-aware algorithms, to implement a ToVF [12], [13]. We have found that these algorithms improve image quality and have benefits with respect to convergence compared to traditional algorithms. In [11] a cost function is developed based on Recursive Least Squares (RLS) which is proposed as an algorithm that can offer benefits in terms of convergence to steady state

as well as reduced complex complexity as long as sparsity can be assumed. Because RLS typically performs better than LMS in terms of image quality at the sacrifice of computational complexity and covergence speed, a modified RLS cost function which can mitigate the drawbacks of traditional RLS is compelling.

2. MATERIALS & METHODS

2.1. Transcranial Ultrasound Imaging

There have been many improvements in TCUI in recent years as researchers have drawn attention to SN hyperechogenicity imaging. The following steps were followed for the imaging to ensure that the results were reliable and reproducible: first, the target structure is placed around the midline of the skull. Second, a sufficient acoustic window is needed for optimal penetration. Third, an increase is needed in echogenicity of the target [2]. The patient is placed in a supine position, and the ultrasound transducer is pressed on the pre-auricular sinus, next to the ear. The clinician sits next to the patient's head and firmly presses the ultrasound transducer to the patients's temporal bone window. The brainstem, ventricles and basal ganglia are imaged on the midline across the patient's brain to be used as "sonographic landmarks". A particular part inside brain structure is identified as hyperechogenic if the planimetrically measured echogenic area is larger than that of 90% of the general population (eg. $0.2\,cm^2$) [2]. The way a clinician determines the size of the echogenic area in the SN is by outlining the area manually with a cursor. However, there are some limitations of TCUI that must be kept in mind. The main limitation is the dependency of TCUI on the size of the bone window. For example, SN hyperechogenicity of Asian people is difficult to measure because of insufficient bone windows in 15 - 60% of individuals [2]. Reliance on the quality of the ultrasound system and the experience of the investigator are other limitations. Clinicians with experience with other applications of B-mode ultrasound can typically be trained more quickly.

2.2. Nonlinear Signal Separation

In order to separate the harmonic components from the unfiltered image, we use the ToVF model to represent the unfiltered input as a sum of the harmonic components which must be solved for. This section shows how to frame the ToVF model in a way such that these components can be solved for using adaptive linear signal processing. The form of the Volterra Filter is as follows:

$$\hat{x}(n + 1) = V_L[x(n)] + V_Q[x(n)] + V_C[x(n)] \quad (1)$$

where the components are

$$V_L = \sum_{i=0}^{N-1} x[n - i]w_L[i]$$

$$V_Q = \sum_{i=0}^{N-1} \sum_{j=0}^{N-1} x[n - i]x[n - j]\, w_Q[i, j]$$

$$V_C = \sum_{i=0}^{N-1} \sum_{j=0}^{N-1} \sum_{k=0}^{N-1} x[n - i]x[n - j]x[n - k]w_C[i, j, k]$$

where in (1), $x(n)$ and $\hat{x}(n + 1)$ are the input and output, respectively. Within the components, V_L, V_Q and V_C are the first, second and third order Volterra operators, and w_L, w_Q and w_C are the linear, quadratic and cubic filter weights, respectively and N denotes the filter length. Generally, Volterra kernels can be complex values. However, only real valued kernels are considered. Noticing that the output is linear with respect to the coefficients, (1) can be rewritten as follows: (note that boldface denotes a vector quantity)

$$\hat{x}(n + 1) = \mathbf{x}^T(n)\, \mathbf{w}_n \quad (2)$$

where the input vector $\mathbf{x}(n)$ is defined as:

$$\begin{aligned} \mathbf{x}(n) \quad = \quad & [x(n), x(n - 1), ..., x(n - N + 1), \quad (3) \\ & x^2(n), x(n)x(n - 1), ..., x^2(n - N + 1), \\ & x^3(n), x^2(n)x(n - 1), ..., x^3(n - N + 1)]^T \end{aligned}$$

and the coefficient vector $\mathbf{w}_n$ is defined as:

$$\begin{aligned} \mathbf{w}_n \quad = \quad & [w_L(0), w_L(1), ..., w_L(N - 1), \quad (4) \\ & w_Q(0, 0), ..., w_Q(N - 1, N - 1), \\ & w_C(0, 0, 0), ..., w_C(N - 1, N - 1, N - 1)]^T \end{aligned}$$

There are three aspects of the Volterra filter that must be pointed out. The first is its ability to suppress Gaussian noise and achieve a signal to noise ratio improvement. Second, it suffers little to no loss within its bandwidth. Third, its output has a linear relationship with its weights. This property is useful when applying minimum mean-square error criterion [10]. Due to its harmonic components, the ToVF can combine a band of frequencies from the fundamental to the second and third harmonic [5].

2.3. Adaptive Recursive Least Square

The adaptive RLS algorithm is one common method used to determine the filter coefficients of the ToVF. The RLS cost function from which our algorithms are derived is as follows:

$$J(n) = \sum_{i=1}^{m} \lambda^{m-i}e(n)^2 + \rho\|\mathbf{w}_n\|_0 \quad (5)$$

where $0 < \lambda < 1$ is the forgetting factor which reduces contribution from previous iterations, ρ is the penalty parameter, $\|\cdot\|_0$ denotes the ℓ_0-norm, which is simply a count of non-zero elements in a vector, and the error is defined as:

$$e(n) = x(n+1) - \mathbf{x}^T(n)\mathbf{w}_n \qquad (6)$$

Because the addition of the ℓ_0-norm constraint makes the minimization of this cost function a non-polynomial problem, a popular approximation for it is:

$$\|\mathbf{w}_n\|_0 \approx \sum_{i=1}^{N-1}(1 - e^{-\beta|w_i|}) \qquad (7)$$

where w_i is the ith element of $\mathbf{w}$, and $|\cdot|$ denotes absolute value. Beta is required to be positive and a strict equality is guaranteed as beta approaches infinity.

The following parameters are derived from (5) and must be updated recursively to implement the algorithms.

$$\mathbf{r}(n) = \lambda\mathbf{r}(n-1) + (1-\lambda)\mathbf{x}(n)\mathbf{x}^T(n)\mathbf{w}_n \qquad (8)$$

$$\mathbf{R}(n) = \lambda\mathbf{R}(n-1) + (1-\lambda)\mathbf{x}(n)\mathbf{x}^T(n) \qquad (9)$$

where $\mathbf{r}(n)$ is an m x 1 matrix, and $\mathbf{R}(n)$ is an m x m matrix, given m is the number of coefficients in the filter. Additionally, $r_i(n)$ is the ith position of $\mathbf{r}$(n), and $R_{i,j}(n)$ is the (i,j)th position of of $\mathbf{R}$(n). The equation that must be solved for the estimation of w_i given n available data, denoted by $\hat{w}_i(n)$, is as follows:

$$R_{i,i}\hat{w}_i(n) = \alpha_i(n) - \rho\beta sgn[\hat{w}_i(n)]e^{-\beta|\hat{w}_i(n)|} \qquad (10)$$

where

$$\alpha_i(n) = r_i(n) - \sum_{j=1}^{i-1}R_{i,j}(n)\hat{w}_j(n) - \sum_{j=i+1}^{N}R_{i,j}(n)\hat{w}_j(n-1) \qquad (11)$$

Equation 10 is nonlinear with respect to $\hat{w}_i(n)$, which makes it difficult to solve without using some approximation. We propose the following two approximations.

2.3.1. STV Approximation

If $\hat{w}_i(n)$ can be assumed to be slow time-varying from one iteration n to the next, then in (10) $e^{\beta|\hat{w}_i(n)|}$ can be approximated by $e^{\beta|\hat{w}_i(n-1)|}$. The solution $\hat{w}_i(n)$ then becomes

$$\hat{w}_i(n) = \frac{sgn[\alpha(n)]}{R_{i,i}(n)}[|\alpha_i(n)| - \rho\beta e^{\beta|\hat{w}_i(n)|}]_+ \qquad (12)$$

where $[x]_+ = max(x,0)$

2.3.2. TSE Approximation

Approximating $e^{-\beta|\hat{w}_i(n)|}$ using it's Taylor Series expansion gives

$$\hat{w}_i(n) = \begin{cases} 1 - \beta x, & |x| < \frac{1}{\beta} \\ 0, & elsewhere \end{cases}$$

Solving for (10) with this approximation gives

$$\hat{w}_i(n) = \begin{cases} \frac{\alpha_i(n)+\rho\beta}{R_{i,i}-\rho\beta^2}, & -\alpha_i^{max}(n) < \alpha_i(n) < -\alpha_i^{min}(n) \\ \frac{\alpha_i(n)-\rho\beta}{R_{i,i}-\rho\beta^2}, & \alpha_i^{min}(n) < \alpha_i(n) < \alpha_i^{max}(n) \\ \frac{\alpha_i(n)}{R_{i,i}}, & |\alpha_i(n)| > \alpha_i^{max}(n) \\ \hat{w}_i(n-1) & elsewhere \end{cases} \qquad (13)$$

where

$$\begin{aligned} \alpha_i^{min}(n) &= min(R_{i,i}(n)/\beta, \rho\beta) \\ \alpha_i^{max}(n) &= max(R_{i,i}(n)/\beta, \rho\beta). \end{aligned}$$

To summarize the procedure, the sequential algorithm is (8),(9), (11), and (12) or (13).

3. RESULTS AND DISCUSSION

The top left image in Figures 1 and 2 was obtained using a Siemens Acuson Sequoia ultrasound system equipped with a Siemens Sequoia 3v2c 64 elements phased array transducer, operating at a frequency of 3 MHz. TCUI was performed through an acoustic window (natural area of reduced bone thickness) in the skull in an early onset human PD patient with a penetration depth of 16 cm. All three algorithms were run with a memory length of $N = 5$. For the STV and TSE algorithms, the parameters ρ and β were set to 1 and 10 respectively. The initializations r(n) and R(n) were

$$\begin{aligned} \mathbf{r}(0) &= 10\rho\beta[1, 1, ..., 1] \\ \mathbf{R}(0) &= \epsilon I \end{aligned} \qquad (14)$$

where ϵ is a small positive constant and I is the identity matrix. All parameters were selected by what has been established in [11] as giving the best performance for this algorithm. The images in Fig. 1 show the cubic component of the image produced by each algorithm, as well as the original B-mode image. As can be seen from the dynamic range bar to the right of each image, the cubic components show an almost similar dynamic range across the three algorithms, all of which are a substantial improvement over the B-mode image. In addition, the reduction of noisy image artifacts is evident when comparing the top left image to the other three. This improvement has been confirmed by the opinions of clinicians who are experts at interpreting these images. Overall, our results

show that the algorithms perform roughly equally in terms of image quality. Also included are the quadratic images in Fig. 2. The ToVF outputs the linear and quadratic components as well as the cubic components which can be useful in cases where a strong response in the second harmonic is expected. In addition, this is identical to the output of a Second Order Volterra filter, which could be desirable if a high memory length is desirable, as the number of coefficients in the ToVF can become prohibitive with large memory lengths. Our results show that the STV and TSE algorithms also perform comparably to RLS in the quadratic images in terms of dynamic range. Fig. 3 shows the learning curve of each algorithm. Both the STV and TSE algorithms converge to steady state more smoothly than RLS. After the second peak in the STV and TSE learning curves, they appear to have converged, whereas RLS is still suffering from spikes in the error. This quick convergence to steady state is especially important in real-time applications.
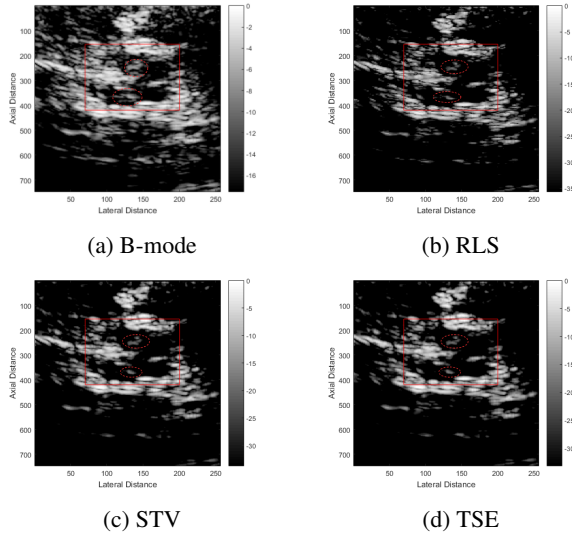

| (a) B-mode | (b) RLS |
| (c) STV | (d) TSE |

Fig. 1: B-mode image (top left), Cubic component of B-mode image obtained using RLS (top right), STV (bottom left), TSE (bottom right). Labeling are in pixels in both directions. The SN is highlighted in red.

4. CONCLUSIONS

We showed that the theoretical benefits of modifying the standard RLS algorithm with an ℓ_0 norm penalty to improve convergence speed can be applicable to *in vivo* applications. The STV and TSE approximations were able to produce comparable image quality to RLS while showing improved convergence speed which means that these algorithms are potentially very well-suited to real-time imaging applications.
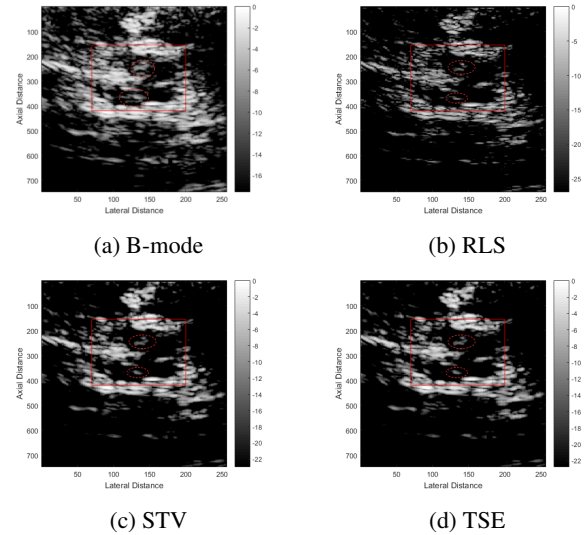

| (a) B-mode | (b) RLS |
| (c) STV | (d) TSE |

Fig. 2: B-mode image (top left), Quadratic component of B-mode image obtained using RLS(top right), STV (bottom left), TSE (bottom right). Labeling are in pixels in both directions. The SN hyperechogenicity is highlighted in red.

5. REFERENCES

[1] T. Subramanian, C. A Lieu, K. Guttalu, and D. Berg, Detection of mptp-induced substantia nigra hyperechogenicity in rhesus monkeys by transcranial ultrasound, Ultrasound in medicine & biology, vol. 36, no. 4, pp. 604-609, 2010.

[2] D. Berg, J. Godau, and U. Walter, Transcranial sonography in movement disorders, The Lancet Neurology, vol. 7, no. 11, pp. 1044-1055, 2008.

[3] D. Berg, Grant, Hyperechogenicity of the substantia nigra: pitfalls in assessment and specificity for Parkinson's disease, Journal of neural transmission, vol. 118, no. 3, pp. 453-461, Springer, 2011.

[4] J. Du, D. Liu, and E. S. Ebbini, Nonlinear imaging of microbubble contrast agent using the volterra filter: In vivo results, IEEE Transactions on Ultrasonics, Ferroelectrics, and Frequency Control, 2016.

[5] P. Phukpattaranont and E. S. Ebbini, Post-beamforming volterra filter for contrast agent imaging, in Engineering in Medicine and Biology Society, 2003. Proceedings of the 25th Annual International Conference of the IEEE. IEEE, 2003, vol. 2, pp. 1172-1175.

[6] H. Yao, P. Phukpattaranont, and E. S Ebbini, Detection and mapping of thermal lesions using dual-mode ultrasound phased arrays, in Ultrasonics Symposium, 2002. Proceedings. 2002 IEEE. IEEE, 2002, vol. 2, pp. 1435-1438.
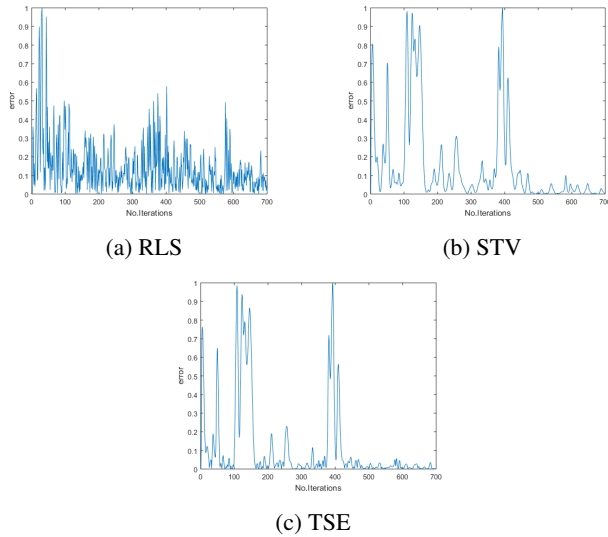
(a) RLS

(b) STV

(c) TSE

Fig. 3: The Learning Curves for each algorithm

[7] E. S. Ebbini, J. C. Bischof, R. K. Visaria, and A. Shrestha, Quadratic b-mode and pulse inversion imaging of thermally-induced lesions in vivo, in 2007 4th IEEE International Symposium on Biomedical Imaging: From Nano to Macro. IEEE, 2007, pp. 1120-1123.

[8] T. Nilmanee and P. Phukpattaranont, Design of a quadratic filter for contrast-assisted ultrasonic imaging based on 2d gaussian filters, Sonklanakarin Journal of Science and Technology, vol. 32, no. 2, pp. 181, 2010.

[9] P. Phukpattaranont, Separation of nonlinear ultrasound signals based on second-order volterra system identification, Japanese Journal of Applied Physics, vol. 48, no. 7S, pp. 07GJ01, 2009.

[10] T. Koh and E. Powers, Second-order volterra filtering and its application to nonlinear system identification, IEEE Transactions on Acoustics, Speech, and Signal Processing, vol. 33, no. 6, pp. 1445-1455, 1985.

[11] K. Shi and P. Shi, Adaptive sparse Volterra system identification with ℓ_0-norm penalty, Signal Processing, vol. 91, no. 10, pp. 2432-2436, 2011.

[12] J. Cunningham, J. Lee, T. Subraminian, M. Almekkawy, Transcranial enhanced ultrasound imaging of induced substantia nigra in brain using adaptive third order Volterra filter: *In-Vivo* results, IEEE International Symposium on Biomedical Imaging, 2017.

[13] *In-Vivo* Transcranial ultrasound Imaging of Induced Substantia Nigra Hyperechogenicity using adaptive sparse third order Volterra filter, IEEE Int. Conference on Neural Engineering, 2017.

[14] D. Berg, R.B Postuma, C.H. Adler, B.R. Bloem, P. chan, B. Dubois, et. al, MDS research criteria for prodromal Parkinsons disease, Movement Disorders, vol. 30, pp. 1600-1611, 2015.

[15] A. Gaenslen, B. Unmuth, J. Godau, I. Liepelt, A. Di Santo, K.J. Schweitzer, et. al, The specificity and sensitivity of transcranial ultrasound in the differential diagnosis of Parkinss disease: a prospective blinded study, Lancet Neurology, vol. 7, no. 5, pp. 417-424, 2008.